Geochemical Perspectives Letters

Magma properties at Earth's lower mantle conditions inferred from electronic structure and coordination in silica

S. Petitgirard, C. Sahle, C. Weiss, K. Gilmore, G. Spiekermann, J.S. Tse, M. Wilke, C. Cavallari, V. Cerantola, C. Sternemann

Supplementary Information

The Supplementary Information includes:

- Experimental Details
- BSE Spectral Calculations
- Data Analysis Details
- Figures S-1 to S-6
- Table S-1
- Supplementary Information References

Experimental Details

X-ray Raman Scattering (XRS) measurements were performed on the ID20 beamline of the ESRF (Grenoble, France) (Huotari *et al*., 2017). The incident energy was set at 9.7 keV through a first high heat-load liquid-nitrogen cooled Si(111) pre-monochromator and a final incident bandwidth of approximately 0.4 eV was obtained using a Si(311) channel-cut post-monochromator. The beam was focused down to ~10×20μm^2 (V x H) through a pair of Kirkpatrick-Baez mirrors. Three out of six spectrometers were used to collect the scattering signal allowing to probe the sample at different transfer momenta $|q|$ up to a maximum of 10Å^{-1}. Each spectrometer contains twelve Si(660) spherically curved crystal analysers that act as focusing monochromator enabling a sub-eV (0.7 eV) final resolution when working at 9.7 keV. The sample was a SiO_2 suprasil glass, the same as for the density measurements (Petitgirard *et al., 2017)*, ground into a fine powder. We used BX90 cells from BGI and PanoDAC or new MBX110 from the ESRF sample environment pool. We performed three measurements through Be gaskets, with cBN inserts, in the PanoDAC following the procedure describe in Sahle *et al*. (2016) using standard conical diamonds with 500 μm culet size and three other measurements up to 100 GPa using 150 μm culet size using the MBX110 DAC from the ESRF pool. For most of the runs we used miniature diamond anvils of about 480 μm thickness (Petitgirard *et al*., 2016), three times thinner than the standard design in order to reduce the absorption of the incoming and scattered X-ray beams (Fig. S-1), with culets of 200 μm up to 66 GPa and 120 μm culet for the highest pressures. The amount of sample was further increased by milling two recesses of 20 μm in the culets of both anvils using a focused ion beam (FIB) at BGI, enabling an increase of sample volume by a factor of three at high pressure. The sample was loaded

into the sample chamber drilled in a 250 μm rhenium gasket pre-indented down to 40 μm thickness with a 100 micron hole and 20 μm thickness and a 60 micron hole for 200 μm culets and 120 μm culets respectively.

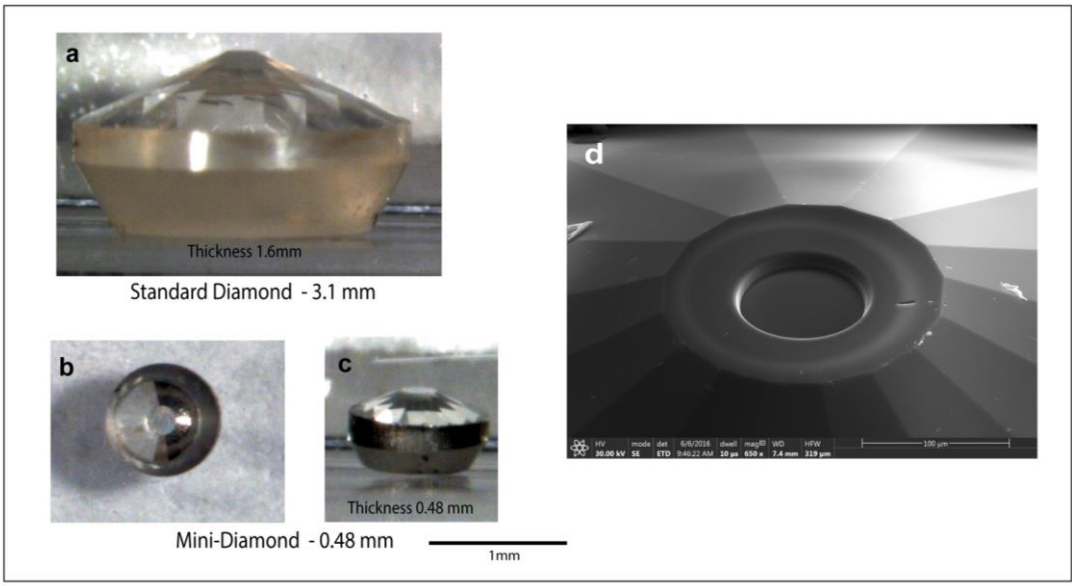

Figure S-1 Miniature diamonds for XRS experiments. **(b-c)** Mini-diamonds dimensions compared to standard diamond anvil **(a). (d)** Milling of a recess using the FIB at BGI Bayreuth.

BSE Spectral Calculations

All spectral calculations were performed on configurations sampled from the previously reported *ab initio* molecular dynamics (MD) simulations of quenched molten quartz (Wu *et al*., 2012) at multiple pressures between ambient and 150 GPa. For all the MD simulations and spectral calculations, the computational cells consisted of 24 structural units (72 atoms). At each pressure, the spectral calculations were based on 10 independent MD configurations and the momentum-dependent Si $L_{2,3}$ and O K-edge XRS spectra were computed as the sum of the excitation spectra of all the Si and O atoms in the structure. For each pressure presented in Figure 1 and Figure S-2, we extracted 10 snapshots at equally spaced time intervals of few ps and evaluated both the Si $L_{2,3}$- and O K-edge for each of the 24 Si and 48 O atoms for a total of 240 individual Si $L_{2,3}$- and 480 O K-edge spectra at each pressure point. The coordination number (CN) was estimated subject to distance cut-off criteria, *i.e.* we used the first minimum in the Si-O radial distribution function as a cut-off and used the number of oxygen atoms around a silicon atom within a sphere with this cut-off radius as the CN.

Calculations of the XRS spectra using the BSE (Bethe-Salpeter Equation) method were performed with the OCEAN code (Obtaining Core level Excitations using *Ab initio* methods and the NIST BSE solver) (Vinson *et al*., 2011). Ground state electron densities and wave functions were generated at the density functional theory (DFT) level using Quantum ESPRESSO (Giannozzi *et al*., 2009). Quantum-ESPRESSO is a community project for high-quality quantum-simulation software, based on density-functional theory, and coordinated by Paolo Giannozzi. See http://www.quantum-espresso.org and http://www.pwscf.org]. Due to the use of pseudopotentials, projector augmented wave (PAW) (Kresse and Joubert, 1998) reconstructed all electron wave functions were generated for the calculation of core to valence transition matrix elements. The dielectric screening was evaluated using a real space implementation of the random phase approximation within a short range, atom centered sphere. Outside this sphere the Levine Louie model dielectric function was used. Results are converged with respect to the change-over radius (Levine and Louie 1982).

Final electron-hole scattering states are obtained by solving the BSE. DFT calculations were performed within the local density approximation (LDA) to the exchange-correlation functional, and using norm conserving pseudopotentials taken from the ABINIT repository. We used FHI formatted pseudopotential from the http://www.abinit.org distribution. A planewave energy cutoff of 70 Ry was used for these calculations. The ground state electron density was calculated using ⊙-point sampling. The wave functions for the screening and BSE calculation were generated from a non-self-consistent-field calculation using a 2x2x2 *k*-point mesh.

Data Analysis Details

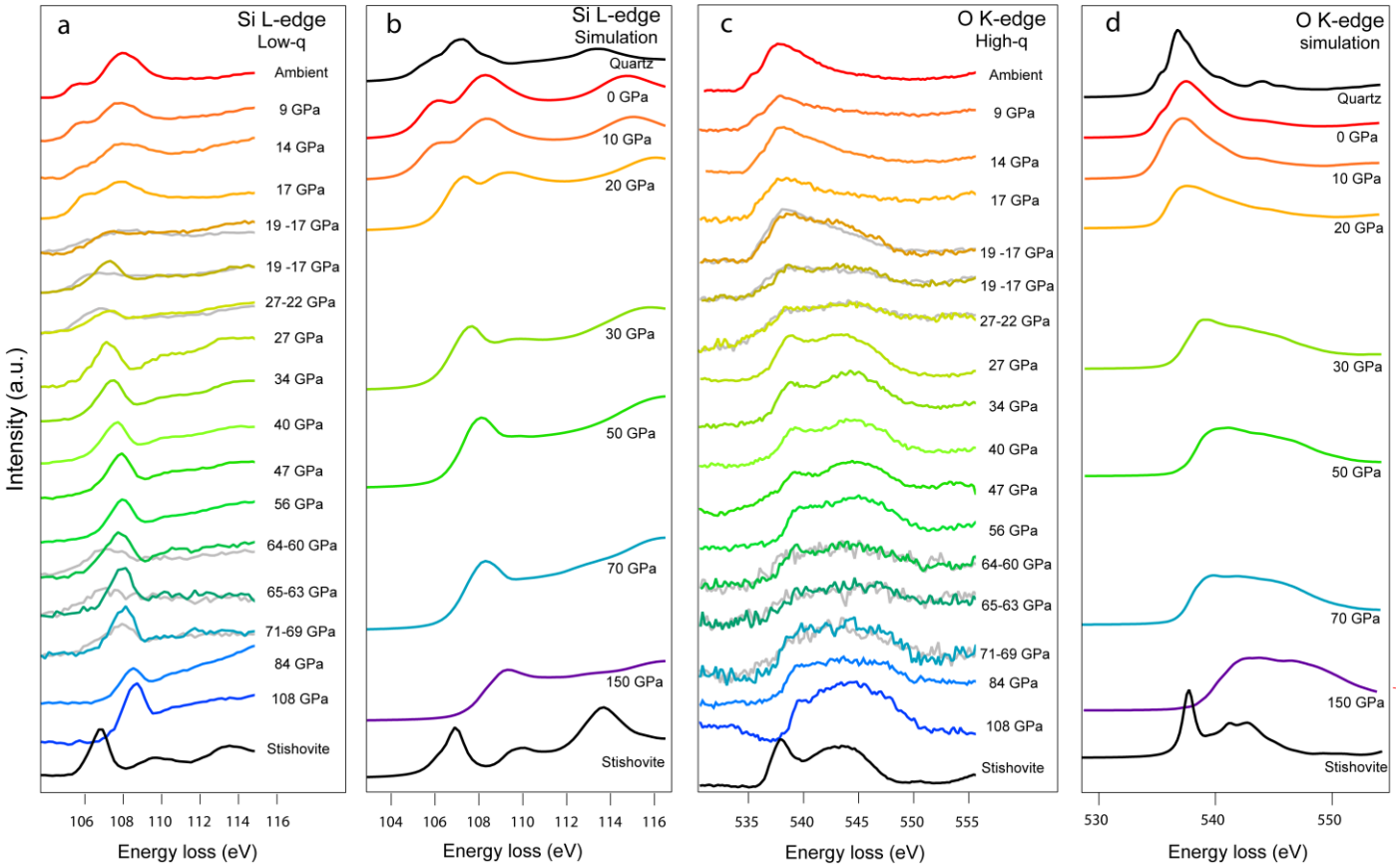

Figure S-2 XRS spectra of the Si $L_{2,3}$ at low-|q| scattering angle **(a)** and O K-edge at high-|q| scattering geometry **(b)** up 110 GPa compared to calculated spectra form MD structures for similar scattering geometry. **(a)** Si $L_{2,3}$ low-|q| measurements compared to calculated spectra in **b**. **(c)** O K-edge measurements at high-|q| compared to calculated spectra in **(d).** Grey spectra in **a** and **c** correspond to the first measurements at the highest pressure indicated on the right, the coloured spectra correspond to the final pressure. More detailed about spectra at pressure around 60 GPa can be found in Figure 4.

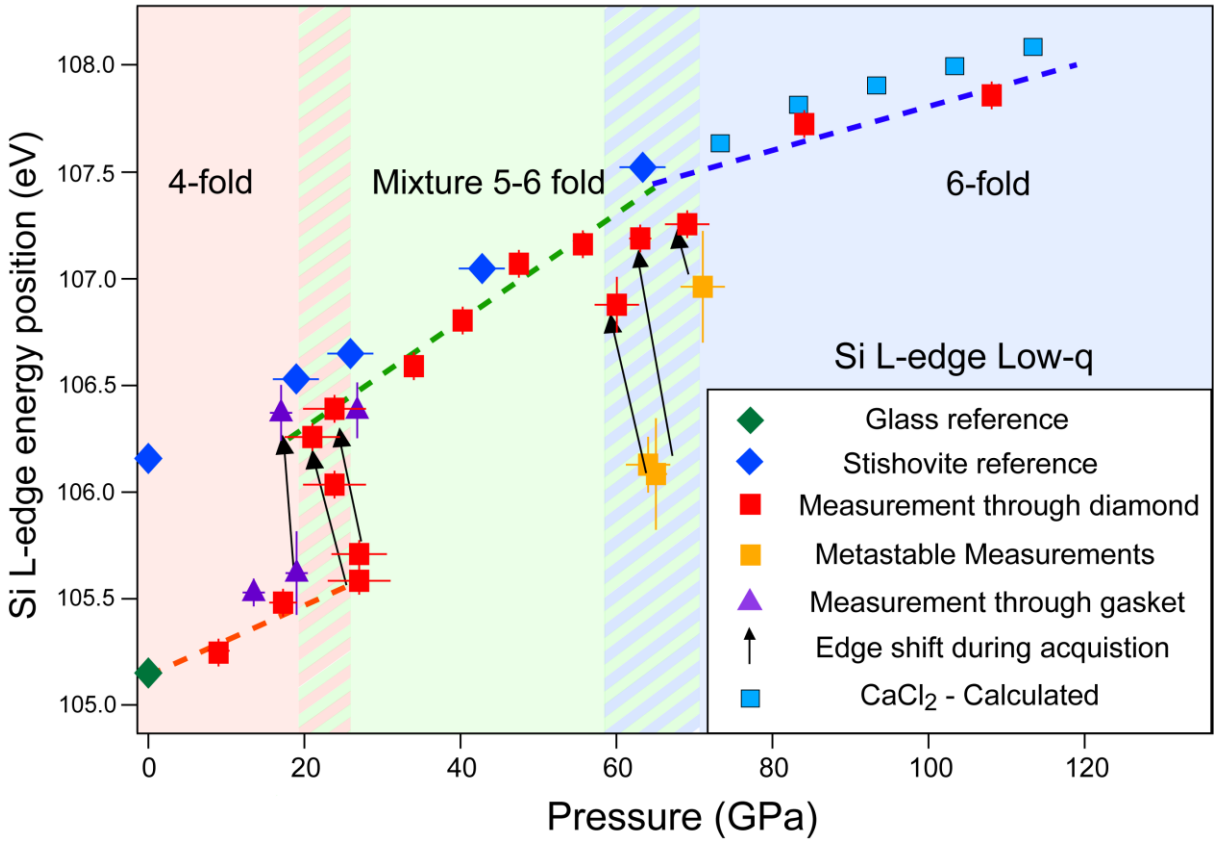

Figure S-3 Silicon edge onset as a function of pressure at low-|q| scattering geometry. As for other scattering geometry at high-|q| but also for the O K-edge, two metastable regions can be observed at ~20 GPa and ~60 GPa corresponding to coordination changes from $^{[4]}$Si to $^{[5/6]}$Si and $^{[5/6]}$Si to $^{[6]}$Si respectively.

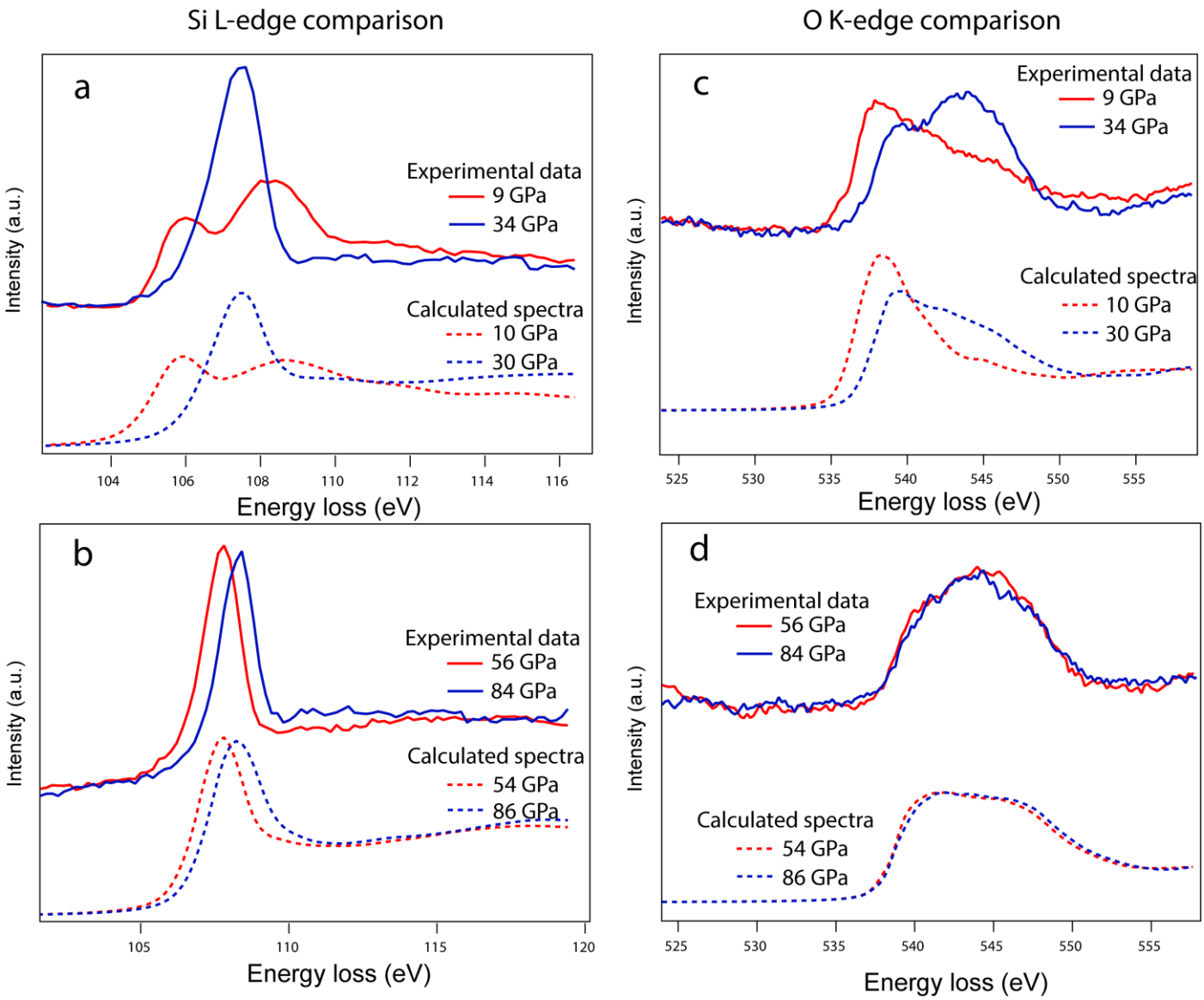

Figure S-4 Comparison between experimental data and calculated spectra from MD structures for the Si L-edge and O K-edge for pressures below and above the main coordination changes at ~20 GPa and ~60 GPa respectively.

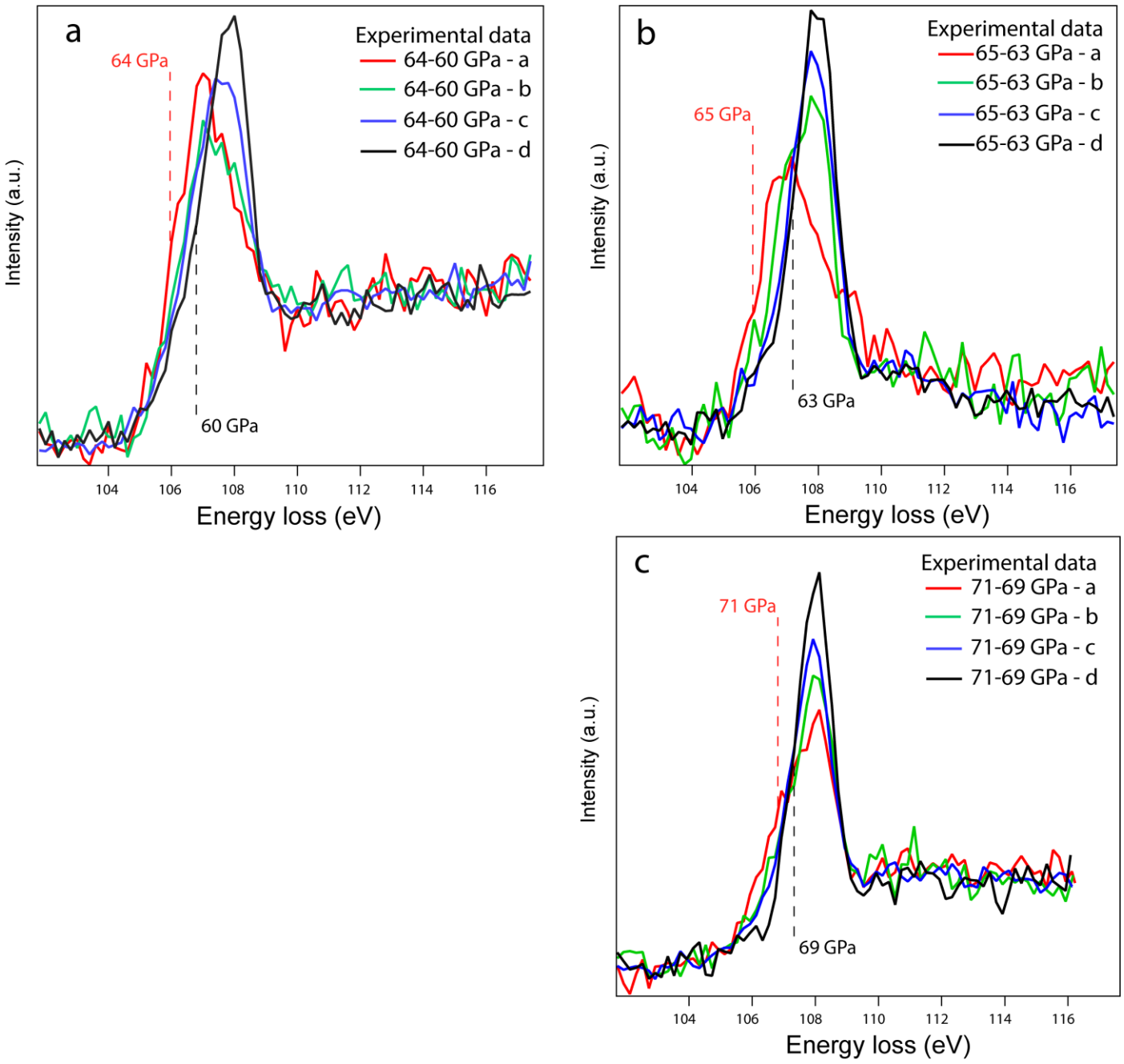

Figure S-5 Si L-edge onset detailed analysis in the metastable region between 60 to 70 GPa for three different pressures and loadings. The four energy scans of the Si L-edge are decomposed and plotted together **(a, b, c).** The pressure of the first spectra in red was measured before and the last pressure in black after the XRS measurement. In **a**, **b** and **c**, the edge onset shifts to higher energy with time while the pressure decreases. The final edge measurements are very close to the value found at lower and higher pressure emphasizing a kinetic effect in the glass for the transition from $^{[5]-[6]}$Si to $^{[6]}$Si. We did not observe such process for other pressure where the edge onset is stable over time as well as the pressure and matches perfectly the calculated spectra (Fig. 3)

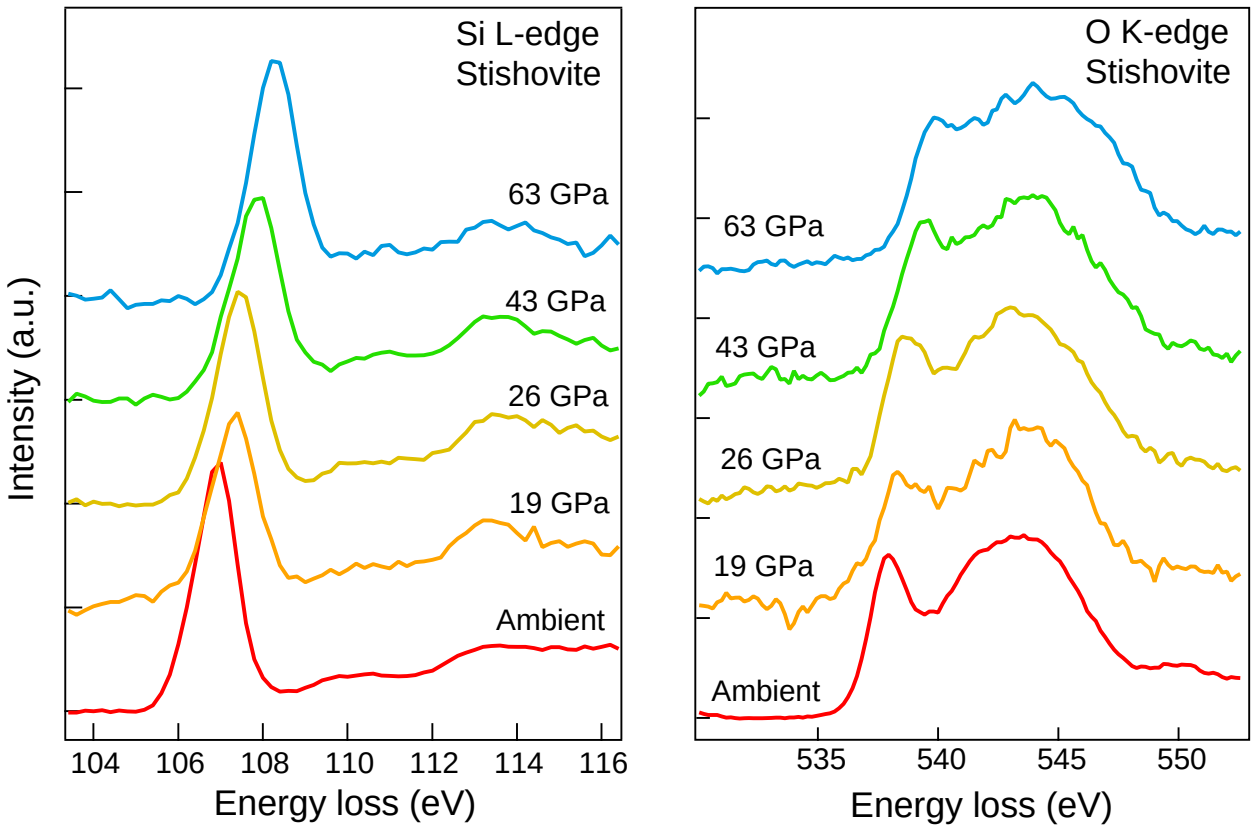

Figure S-6 XRS measurements of the Si L-edge and O K-edge of stishovite reference material under high pressure up to 63 GPa

Table S-1 Data for the edge onset measurements for both the Si L-edge and O K-edge as a function of pressure as well as reference material values for stishovite and glass. In the table, all the data collected in different geometry (through Be and through the diamonds) are reported. The bold italic numbers correspond to edge onset and pressure values of the two transitions where the spectra are changing during the measurement (around 20 GPa and 60 GPa). All other points were stable over time.

Geometry	Pressure	Si Edge Onset	Geometry	Pressure	O Edge Onset
Through Be	14.00	105.17	*Through Be*	14.00	536.56
	19.00	***105.31***		***19.00***	***536.67***
	17.00	***105.79***		***17.00***	***536.75***
	26.75	106.20		26.75	537.39
Through Diamond	9.00	105.09	*Through Diamond*	9.00	536.48
	17.25	105.24		17.25	536.57
	27.00	***105.37***		***27.00***	***536.47***
	23.85	***105.77***		***23.85***	***537.14***
	23.85	***106.20***		***23.85***	***537.37***
	27.00	***105.59***		***34.00***	***537.73***
	22.00	106.08		40.25	538.12
	34.00	106.44		47.45	538.37
	40.25	106.64		55.65	538.58
	47.45	106.90		62.00	538.18
	55.65	107.02		64.00	538.35
	62.00	106.77		69.00	538.37
	64.00	107.06		84.00	538.79
	69.00	107.14		108.00	538.87
	84.00	107.57			
	108.00	107.76			
Metastable region	***63.00***	***105.91***	*Metastable region*	***63.00***	***537.10***
	62.00	***106.04***		***62.00***	***536.46***
	61.00	***106.38***		***61.00***	***538.03***
	65.00	***105.92***		***65.00***	***536.86***
	64.00	***106.51***		***64.00***	***538.81***
	63.00	***106.88***		***63.00***	***538.41***
	70.00	***106.49***		***70.00***	***538.10***
	68.00	***107.05***		***68.00***	***537.97***
	68.00	***107.03***		***68.00***	***538.14***
Reference			**Reference**		
Stishovite	0.00	105.99	*Stishovite*	0.00	536.94
Glass	0.00	104.91	*Glass*	0.00	536.29
Stishovite	0.00	105.99	*Stishovite*	0.00	536.94
	19.00	106.41		19.00	537.38
	26.00	106.52		26.00	537.62
	43.00	106.90		43.00	538.22
	63.00	107.35		63.00	538.77

Supplementary Information References

Giannozzi, P. *et al.* (2009) QUANTUM ESPRESSO: a modular and opensource software project for quantum simulations of materials. *Journal of Physics Condensed Matter* 21, 395502.

Kresse, G., Joubert, D. (1998) From ultra-soft pseudopotentials to the projector augmented-wave method. *Physical Review B* 59, 1758.

Levine, Z.H., Louie, S.G. (1982) New model dielectric function and exchange correlation potential for semiconductors and insulators. *Physical Review B* 25, 6310.

Huotari, S. *et al.* (2017) A large-solid-angle X-ray Raman scattering spectrometer at ID20 of the European Synchrotron Radiation Facility. *Journal of Synchrotron Radiation 24*, 521–530.

Petitgirard, S. *et al.* (2016) Miniature Diamond Anvils for X-Ray Raman Scattering Spectroscopy Experiments at High Pressure. *Journal of Synchrotron Radiation* 24, 276–282

Petitgirard, S. *et al.* (2017) SiO2 Glass Density to Lower-Mantle Pressures. *Physical Review Letters* 119, 215701.

Sahle, C.J. *et al.* (2016) Direct tomography imaging for inelastic x-ray scattering experiments at high pressure. *Journal of Synchrotron Radiation* 24, 269–275.

Wu, M., Liang, Y., Jiang, J.-Z., Tse, J.S. (2012) Structure and Properties of Dense Silica Glass. *Scientific Reports* 2, 398.

Vinson, J., Rehr, J.J., Kas, J.J., Shirley, E.L. (2011) Bethe-Salpeter equation calculations of core excitation spectra. *Physical Review B* 83, 115106.